HAL open science

Generic elasticity of thermal, under-constrained systems

Cheng-Tai Lee, Matthias Merkel

▶ To cite this version:

Cheng-Tai Lee, Matthias Merkel. Generic elasticity of thermal, under-constrained systems. 2023. hal-04251707

HAL Id: hal-04251707

https://hal.science/hal-04251707v1

Preprint submitted on 20 Oct 2023

HAL is a multi-disciplinary open access archive for the deposit and dissemination of scientific research documents, whether they are published or not. The documents may come from teaching and research institutions in France or abroad, or from public or private research centers.

L'archive ouverte pluridisciplinaire **HAL**, est destinée au dépôt et à la diffusion de documents scientifiques de niveau recherche, publiés ou non, émanant des établissements d'enseignement et de recherche français ou étrangers, des laboratoires publics ou privés.

Distributed under a Creative Commons Attribution 4.0 International License

arXiv:2304.07266v1 [cond-mat.soft] 14 Apr 2023

Generic elasticity of thermal, under-constrained systems

Cheng-Tai Lee and Matthias Merkel*
Aix Marseille Univ, Université de Toulon, CNRS, CPT (UMR 7332),
Turing Center for Living Systems, Marseille, France
(Dated: April 17, 2023)

Athermal (i.e. zero-temperature) under-constrained systems are typically floppy, but they can be rigidified by the application of external strain, which is theoretically well understood. Here and in the companion paper, we extend this theory to *finite* temperatures for a very broad class of under-constrained systems. In the vicinity of the athermal transition point, we derive from first principles expressions for elastic properties such as isotropic tension t and shear modulus G on temperature T, isotropic strain ε, and shear strain γ, which we confirm numerically. These expressions contain only three parameters, which depend on the microscopic structure of the system. These respectively describe entropic rigidity, energetic rigidity, and an interaction between isotropic and shear strain. Our results imply that in under-constrained systems, entropic and energetic rigidity interact like two springs in series. This also allows for a simple explanation of the previously observed scaling relation $t \sim G \sim T^{1/2}$ at $\varepsilon = \gamma = 0$. Our work unifies the physics of systems as diverse as polymer fibers & networks, membranes, and vertex models for biological tissues.

Understanding rigidity of amorphous materials still represents a fundamental challenge, which is relevant for questions ranging from the glass transition in inert materials [1] to solid-fluid transitions in living systems [2].

In the athermal limit, i.e. at zero temperature, the rigidity of many systems, including spring networks and particulate matter, can be predicted using Maxwell-Calladine constraint counting [3–6]. In this approach, one compares the number of constraints, N_s (e.g. the number of springs in a spring network), to the number of degrees of freedom, $N_{\rm dof}$ (e.g. the node positions in a spring network). Roughly, if $N_s > N_{\rm dof}$, the system is expected to be rigid. Conversely, if $N_s < N_{\rm dof}$, the system is under-constrained and expected to be floppy.

However, it is known that even under-constrained systems can be rigidified [4, 7–12]. This occurs for instance when there is geometric incompatibility between spring rest lengths and externally applied strain. For example, in the simple spring network in Fig. 2b, we illustrate what happens when progressively increasing the externally applied isotropic strain ε while keeping the spring rest lengths fixed. Eventually, as ε is increased above a critical value, here for convenience defined as the point of zero strain, $\varepsilon = 0$, the springs necessarily need to be stretched. At the boundary of geometric incompatibility ($\varepsilon = 0$), a so-called state of self-stress (SSS) emerges [6]. This means that specific combinations of virtual tensions can be put on the springs without resulting in any net forces on any of the (movable) nodes. In previous work, we used the properties of the SSS created at the

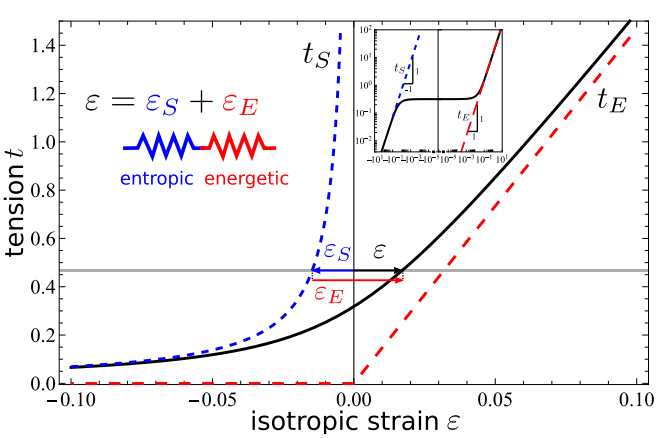

FIG. 1. Analytical predictions for the isotropic tension t depending on isotropic strain ε, shown for the athermal limit (red dashed line), the infinitely-stiff-spring limit (blue dashed line), and the general case of finite spring stiffness and temperature (black solid line). (inset) Same plot in log-log scaling.

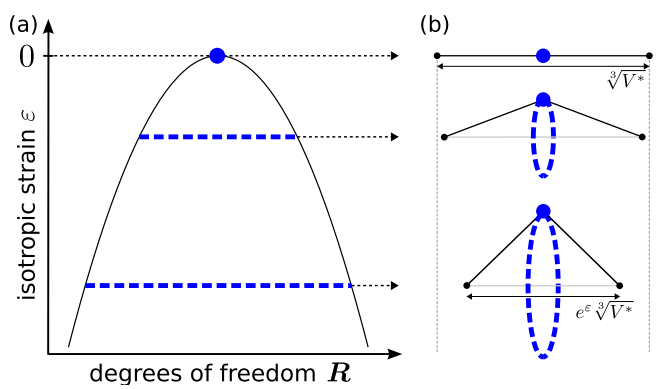

FIG. 2. (a) Schematic: Variation of the accessible phase space volume Ω with isotropic strain ε in the limit of infinitely stiff springs. Starting at the athermal transition point at $\varepsilon = 0$, upon isotropic compression ($\varepsilon < 0$), Ω is expected to increase with the distance $|\varepsilon|$ to the athermal transition point. The abscissa represents the $N_{\rm dof}$-dimensional configuration space. (b) Illustration of a simple two-spring system in 3D of linear dimension $\sqrt[3]{V} = e^{\varepsilon}\sqrt[3]{V^*}$, where the black nodes have fixed positions and the blue node is freely movable. In panels a and b, blue dashed lines represent the accessible parts of the phase space.

rigidity transition to analytically derive the elastic properties in the athermal limit [9, 13]. Our approach applies not only to spring networks, but also to other systems such as polymer networks [14–17] and vertex models for biological tissues [9, 10, 18–20].

While we analytically understand rigidity in the athermal limit, there are mostly only numerical results for the case of a finite temperature, i.e. for *thermal* under-constrained systems [21–25]. For instance, previous studies showed numerically that upon increasing temperature T from the athermal rigidity transition point, the shear modulus G scales as $G \sim T^{1/2}$ [22, 23]. For specific spring networks, this scaling could be derived analytically using effective-medium theory (EMT) before [26], but a derivation from first principles independent from the assumptions inherent to EMT has been lacking so far. There is also work treating a related abstract constraint satisfaction problem using the replica approach [27], work studying these questions in isostatic or over-constrained systems [26, 28–30], and work discussing the effect of singularities on under-constrained systems [31]. However, despite these advances, we still miss a general understanding for the elastic properties of thermal, under-constrained systems, in particular their response to isotropic and shear strain.

Here and in the companion paper [32], we develop a generic analytical theory for thermal, under-constrained systems in the vicinity of the athermal transition point. We first derive the elastic system properties in the limit of infinitely stiff springs, where only entropic elasticity plays a role. To then discuss the general case of finite spring stiffness and finite temperature (black solid line in Fig. 1), we then combine the stiff-spring results (blue dashed line) with our earlier results for the athermal limit, where only energetic elasticity plays a role (red dashed line) [9, 13]. We provide an intuition for why the system behaves as if the two limiting cases were "put in series", i.e. entropic and energetic strains add up (illustration in Fig. 1). Finally, we test our analytical results numerically, using simulations of randomly cut triangular networks. With only three fit parameters, our analytical results reproduce the observed behavior of tension t and shear modulus G over many orders of magnitude of varying isotropic strain ε, shear strain γ, and temperature T.

To discuss the key ideas of our approach, we focus here on an under-constrained network of linear springs with equal spring constants K and rest lengths L_0. The more general case of varying spring constants and rest lengths is discussed in the companion paper [32]. The system energy is:

$$E = \frac{K}{2} \sum_{i=1}^{N_s} (L_i - L_0)^2, \tag{1}$$

where the sum is over all springs i. The length L_i of spring i depends on isotropic strain ε, shear strain γ, and the positions $\boldsymbol{R}_a$ of the nodes it connects, where a is the node index. We use periodic boundary conditions in D spatial dimensions with periodic box volume V. Isotropic strain ε is defined as linear strain, i.e. $V = e^{D\varepsilon} V^*$, where V^* is the system volume at the athermal transition point. Shear strain γ can be either pure shear strain, or simple shear strain using Lees-Edwards-like boundary conditions [33].

It will be convenient to consider geometric quantities that are rescaled with respect to system size. For instance, we consider the rescaled node positions $\boldsymbol{r}_a := V^{-1/D} \boldsymbol{R}_a = e^{-\varepsilon} (V^*)^{-1/D} \boldsymbol{R}_a$. Because the springs in our network are linear, the spring lengths are homogeneous with respect to isotropic strain. Thus, the rescaled spring lengths $\ell_i(\{\boldsymbol{r}_a\}, \gamma) := e^{-\varepsilon} L_i(\{\boldsymbol{R}_a\}, \varepsilon, \gamma)/L_0$ do not depend on isotropic strain ε any more.

In the athermal limit, the elastic properties arise from purely energetic interactions, and their analytical expressions have been derived before [9, 13]. Briefly, for small isotropic and shear strain, the system is rigid for $\varepsilon + b_\varepsilon \gamma^2 > 0$, where b_ε is a constant that depends on the microscopic network structure. In the rigid regime close to the transition, energetically created isotropic tension t_E and shear modulus G_E are given by (red dashed line in Fig. 1) [32]:

$$t_E = \kappa_E \big(\varepsilon + b_\varepsilon \gamma^2\big) \tag{2}$$

$$G_E = 2D b_\varepsilon \kappa_E \big(\varepsilon + 3 b_\varepsilon \gamma^2\big), \tag{3}$$

where κ_E is a constant that depends on the microscopic network structure.

In the thermal case, the configurational degeneracy of the system becomes important (Fig. 2). To discuss its influence, we first consider the stiff-spring limit, $K \to \infty$, which implies a hard constraint for all spring lengths: $L_i = L_0$. To sketch the derivation of the elastic system properties in this limit we set for simplicity $\gamma = 0$ here. The general case including γ is described in the companion paper [32]. To derive how the accessible phase space volume Ω scales with ε, we first note that the spring length constraints $L_i = L_0$ link the rescaled spring lengths ℓ_i to isotropic strain ε: To linear order in ε, the definition of ℓ_i implies: $\Delta\ell_i := \ell_i - 1 = -\varepsilon$. We then Taylor-expand all rescaled spring lengths around the transition:

$$-\varepsilon \equiv \Delta\ell_i = C_{in} \Delta r_n + \frac{1}{2} M_{imn} \Delta r_m \Delta r_n, \tag{4}$$

where we use Einstein notation (implied sum over equal indices). We introduced $\Delta r_n := r_n - r_n^*$, where the r_n with $n = 1, \ldots, N_{\mathrm{dof}}$ correspond to all components of the rescaled node positions $\boldsymbol{r}_a$, and r_n^* denotes their respective values at the transition point. The matrix C_{in} is the compatibility matrix at the transition point, and M_{imn} is the second spring length derivative at the transition point. Performing a singular-value decomposition

on C_{in}, we can express Eq. (4) in terms of the "eigen modes" of C_{in}:

$$-\varepsilon\tilde{w}_p = s_{\underset{\cdot}{p}}\Delta\tilde{r}_{\underset{\cdot}{p}} + \frac{1}{2}\tilde{M}_{pmn}\Delta\tilde{r}_m\Delta\tilde{r}_n, \tag{5}$$

where the s_p with $p = 1, \ldots, N_s$ are the singular values of C_{in}, indices with underdot are not summed over, and the quantities with tilde were transformed into the respective "eigen space" of C_{in}. In particular, the N_s-dimensional vector $(\tilde{w}_p)$ corresponds to the N_s-dimensional vector $(w_i) = (1, \ldots, 1)$ transformed into the eigen space of C_{in}. In general, in disordered networks, a single SSS is created at the transition point [6, 9]. Sorting the s_p in decreasing order, we thus have that $s_p > 0$ for $p < N_s$ and $s_{N_s} = 0$.

Retaining only the lowest-order terms in ε, we obtain from Eq. (5) after some discussion [32]:

$$-\varepsilon\tilde{w}_p = s_{\underset{\cdot}{p}}\Delta\tilde{r}_{\underset{\cdot}{p}} + \frac{1}{2}\sum_{m,n=N_s}^{N_{\rm dof}}\tilde{M}_{pmn}\Delta\tilde{r}_m\Delta\tilde{r}_n \quad \text{for } p = 1, \ldots, N_s. \tag{6}$$

Each of these N_s equations includes all the $\Delta\tilde{r}_n$ with $n \geq N_s$. However, each of the $\Delta\tilde{r}_p$ with $p < N_s$ appears only once in total; as linear terms in the equation with index p. Thus, for a given value of ε, the first $N_s - 1$ equations only fix the values of the $\Delta\tilde{r}_p$ with $p < N_s$. Meanwhile, the last equation, $p = N_s$, puts a constraint on the $\Delta\tilde{r}_n$ with $n \geq N_s$. Because $s_{N_s} = 0$, this equation describes the surface of a hyper-ellipsoid (compare Fig. 2b) whose half axes scale as $\sim \sqrt{-\varepsilon}$. Some of the eigen values of the matrix $\tilde{M}_{N_s mn}$ are zero; for instance those that correspond to a global translation of all nodes. The ellipsoid is thus N_e-dimensional, where N_e is the number of non-zero eigen values of $\tilde{M}_{N_s mn}$, which fulfills $N_e \leq N_{\rm dof} - N_s - D + 1$. Thus, the surface of the ellipsoid scales as $\sim (-\varepsilon)^{(N_e-1)/2}$. Together with an additional prefactor of $\sim 1/\sqrt{-\varepsilon}$ due to the constraint on the spring lengths [32], we obtain for the accessible phase space volume:

$$\Omega \sim (-\varepsilon)^{\frac{N_e-2}{2}}. \tag{7}$$

The free energy consists only of an entropic contribution $F_S = -k_B T \log\Omega = -k_B T([N_e - 2]/2)\log[-(\varepsilon + b_\varepsilon\gamma^2)]$, where k_B denotes the Boltzmann constant, and we neglected constant offsets. Also, we have included the dependency on γ, which we derive in the companion paper [32]. We thus obtain for the purely entropic tension $t_S = (\partial F_S/\partial\varepsilon)/V$ and shear modulus $G_S = (\partial^2 F_S/\partial\gamma^2)/V$:

$$t_S = -\frac{\kappa_S T}{\varepsilon + b_\varepsilon\gamma^2} \tag{8}$$

$$G_S = -2Db_\varepsilon\kappa_S T\frac{\varepsilon - b_\varepsilon\gamma^2}{(\varepsilon + b_\varepsilon\gamma^2)^2}, \tag{9}$$

with $\kappa_S = k_B(N_e - 2)/2DV^*$. Hence, not only energetic rigidity [9, 13], but also entropic rigidity is determined by the properties of the SSS that is created at the athermal transition point.

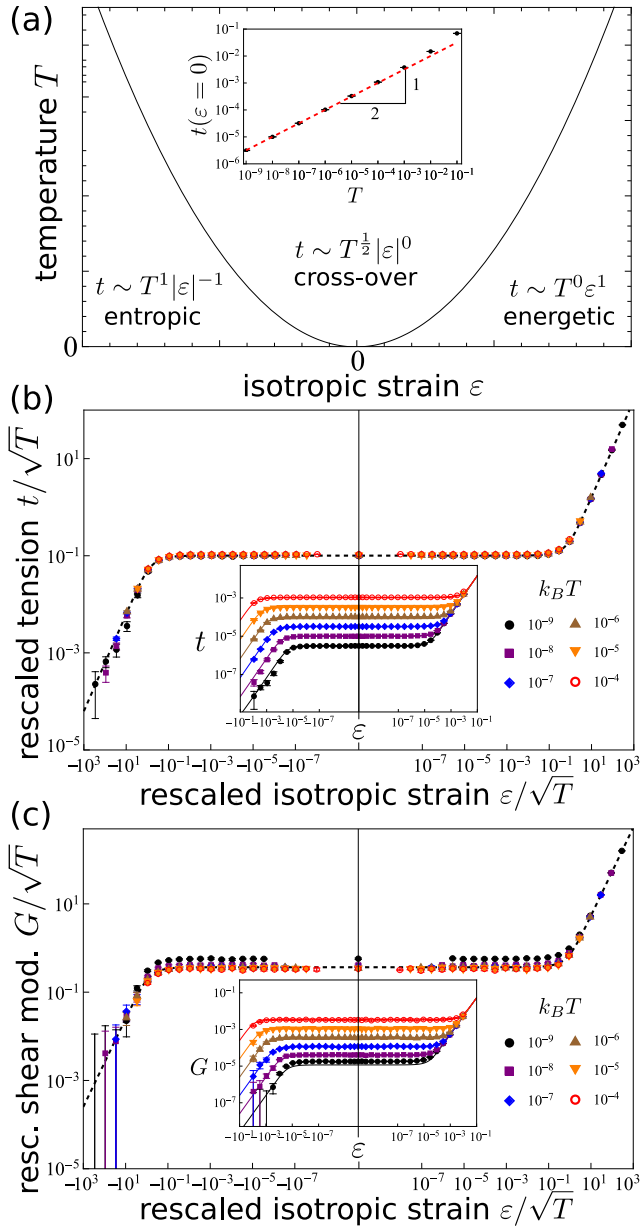

FIG. 3. Numerical results for zero shear strain, $\gamma = 0$. (a) We find three scaling regimes. (a inset) For $\varepsilon = 0$, we numerically confirm the scaling $t \sim T^{1/2}$. The red dashed line is a fit to the curve $t = \sqrt{\kappa_E\kappa_S T}$ for $T \leq 10^{-6}$ to extract the value of $\sqrt{\kappa_E\kappa_S}$. (b,c) When plotting isotropic tension t (b) or shear modulus G (c) over isotropic strain ε, a rescaling by $\sqrt{T}$ leads to a collapse of the curves for the different temperatures. (respective inset) Same data without rescaling. All curves in panels b, c and their insets are predictions from Eqs. (11) and (12) using a single parameter set $(\kappa_E, \kappa_S, b_\varepsilon)$ [34].

For $\gamma = 0$, the scaling of the tension is plotted in Fig. 1 (blue dashed line). This scaling is consistent with known results for some under-constrained systems. For instance,

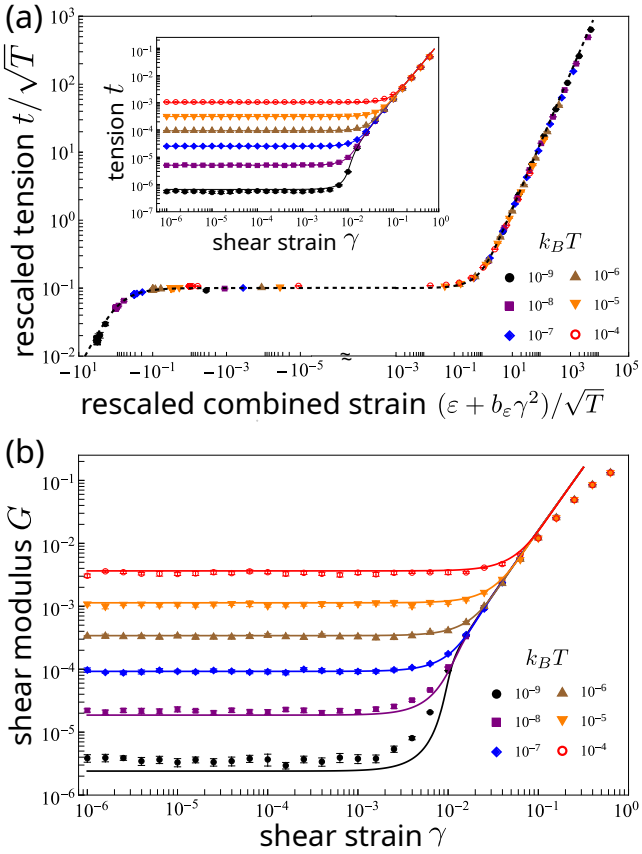

FIG. 4. Numerical results for varying shear strain, $\gamma > 0$, with fixed $\varepsilon = -9.15 \times 10^{-5}$. (a) When plotting isotropic tension t over the combined strain, $\varepsilon + b_\varepsilon\gamma^2$, a rescaling by $\sqrt{T}$ leads to a collapse of the curves for the different temperatures. (a inset) Same data without rescaling, and on the x axis shear strain is plotted directly. (b) Shear modulus G over shear strain γ. All curves are predictions from Eqs. (11) and (12) using the same parameter set as in Fig. 3.

the tension of a freely jointed chain scales as $\sim -T/\varepsilon$ close to the fully stretched chain configuration [35], and so does the tension of an incompressible membrane without bending rigidity close to the fully stretched state [36].

We now discuss the general case of finite spring stiffness K and finite temperature T, where entropic and energetic elasticity compete with each other. Entropic effects generally tend to elongate individual springs in order to increase the phase space volume, but strongly elongated springs are less favorable energetically. To get a more quantitative intuition for the interplay between entropic and energetic elasticity, we consider boundary conditions that ensure $\gamma = 0$ and constant tension $t > 0$ (horizontal gray line in Fig. 1). In the thermal stiff-spring limit, $K \to \infty$, this leads to a negative strain $\varepsilon_S < 0$ (blue arrow), which is according to Eq. (8): $\varepsilon_S = -\kappa_S T/t$ (blue dashed line). When we now allow for a finite spring constant K, the springs additionally stretch, increasing the total strain by some amount ε_E to the total strain $\varepsilon = \varepsilon_S + \varepsilon_E$ (red and black arrows, respectively). For sufficiently small temperatures, the network geometry is on average not very different from the athermal network. So, using Eq. (2), we have $\varepsilon_E = t/\kappa_E$ (red dashed line). Thus, the total strain depends on tension as (black solid line)

$$\varepsilon = -\frac{\kappa_S T}{t} + \frac{t}{\kappa_E}. \tag{10}$$

In other words, the interaction between entropic and energetic elasticity corresponds to an entropic and an energetic spring acting in series (Fig. 1). The rigorous analysis in our companion paper confirms that this intuitive explanation leads to the exact result for $N_e \gg 1$ [32].

Inverting Eq. (10) we find:

$$t = \frac{\kappa_E}{2}\left(\varepsilon + b_\varepsilon\gamma^2 + \left|\varepsilon + b_\varepsilon\gamma^2\right|\sqrt{1+\theta}\right), \tag{11}$$

where $\theta := 4\kappa_S T/[\kappa_E(\varepsilon + b_\varepsilon\gamma^2)^2]$. The γ dependency that we have included here is derived in the companion paper [32]. We find for the shear modulus [32]:

$$G = 2Db_\varepsilon t\left[1 + \frac{2b_\varepsilon\gamma^2}{|\varepsilon + b_\varepsilon\gamma^2|\sqrt{1+\theta}}\right]. \tag{12}$$

Thus, the shear modulus is proportional to tension for $\gamma = 0$, but not for varying γ.

Our approach also provides a simple explanation for the previously observed $G \sim T^{1/2}$ scaling for $\varepsilon = 0$ and $\gamma = 0$. In this limit, we find from Eqs. (11) and (12) that $t = \sqrt{\kappa_E\kappa_S T}$ and $G = 2Db_\varepsilon t$. The relation for t can also be obtained immediately from Eq. (10) with $\varepsilon = 0$.

More generally, we find three scaling regimes, which we discuss here for $\gamma = 0$ (Fig. 3a and inset to Fig. 1). (i) For $\theta \ll 1$ and $\varepsilon < 0$, the system behaves like in the stiff-spring limit with $G \sim t \sim T^1|\varepsilon|^{-1}$. (ii) For $\theta \ll 1$ and $\varepsilon > 0$, the system behaves like in the athermal regime with $G \sim t \sim T^0\varepsilon^1$. (iii) For $\theta \gg 1$, the system shows the scaling $G \sim t \sim T^{1/2}\varepsilon^0$. This is remarkably analogous to previous results [26], where strain is replaced by the network connectivity. We discuss a possible reason for this in the companion paper [32].

We tested our analytical results using Monte-Carlo (MC) simulations of a 2D under-constrained randomly cut triangular network in periodic boundary conditions [37]. We first set shear strain to zero, $\gamma = 0$, varying only isotropic strain ε and temperature T (Fig. 3). We confirmed the $t \sim T^{1/2}$ scaling for $\varepsilon = 0$ (inset to Fig. 3a). Furthermore, Eqs. (11) and (12) predict that for $\gamma = 0$ the tension-strain and shear-modulus-strain curves respectively collapse when rescaling each of t, G, and ε by $\sqrt{T}$, which we confirm numerically in Fig. 3b,c. The theoretical predictions are shown as dashed and solid curves, where the values of κ_E, κ_S, and b_ε were obtained independently, from data at $T = 0$ and at $\varepsilon = 0$ [34]. Note that the value of κ_S can also directly be obtained from

N_e, by counting the non-zero eigen values of $\tilde{M}_{N_s mn}$ with $m, n \geq N_s$. Indeed, for our network studied here, we find $N_e = 433$, which is consistent with the observed value for κ_S [34].

We further tested our analytical results for varying shear strain, $\gamma > 0$, fixing isotropic strain ε (Fig. 4). For the tension t, Eq. (11) again implies a scaling collapse onto a theoretical curve, which we confirm numerically in Fig. 4a. The solid and dashed lines in Fig. 4a and inset indicate again the prediction according to Eq. (11), using the same parameter values as before [34]. Similarly, the shear modulus data follows the analytical prediction in Eq. (12) (Fig. 4b). Deviations in the shear modulus at the lowest temperature are consistent with slightly insufficient equilibration, and deviations at larger shear strain are likely due to higher-order terms.

In conclusion, we have developed a generic analyical theory for the elastic properties of thermal, underconstrained systems, and their behavior under isotropic and shear strain. We expect this work to unify the physics of a broad class of materials, including polymer fibers, polymer networks, membranes, and vertex models for biological tissues.

We thank Chris Santangelo, Jen Schwarz, and Manu Mannattil for fruitful discussions. We thank the Centre Interdisciplinaire de Nanoscience de Marseille (CINaM) for providing office space. The project leading to this publication has received funding from France 2030, the French Government program managed by the French National Research Agency (ANR-16-CONV-0001), and from the Excellence Initiative of Aix-Marseille University - A*MIDEX.

* matthias.merkel@cnrs.fr

[1] P. Charbonneau, J. Kurchan, G. Parisi, P. Urbani, and F. Zamponi, Annual Review of Condensed Matter Physics **8**, 265 (2017), arxiv:1605.03008.
[2] P.-F. Lenne and V. Trivedi, Nature Communications **13**, 1 (2022).
[3] J. C. Maxwell, Philosophical Magazine Series 4 **27**, 294 (1864).
[4] C. R. Calladine, International Journal of Solids and Structures **14**, 161 (1978).
[5] A. J. Liu and S. R. Nagel, Annual Review of Condensed Matter Physics **1**, 347 (2010).
[6] T. C. Lubensky, C. L. Kane, X. Mao, A. Souslov, and K. Sun, Reports on Progress in Physics **78**, 73901 (2015), arxiv:1503.01324.
[7] S. Alexander, Physics Report **296**, 65 (1998), arxiv:1512.04885.
[8] B. Cui, G. Ruocco, and A. Zaccone, Granular Matter **21**, 69 (2019), arxiv:1901.09582.
[9] M. Merkel, K. Baumgarten, B. P. Tighe, and M. L. Manning, Proceedings of the National Academy of Sciences **116**, 6560 (2019).
[10] M. Moshe, M. J. Bowick, and M. C. Marchetti, Physical Review Letters **120**, 268105 (2017), arxiv:1708.07848.
[11] O. K. Damavandi, V. F. Hagh, C. D. Santangelo, and M. L. Manning, Physical Review E **105**, 025004 (2022).
[12] S. Zhang, E. Stanifer, V. V. Vasisht, L. Zhang, E. Del Gado, and X. Mao, Physical Review Research **4**, 043181 (2022).
[13] C.-T. Lee and M. Merkel, Soft Matter **18**, 5410 (2022).
[14] P. R. Onck, T. Koeman, T. van Dillen, and E. van der Giessen, Physical Review Letters **95**, 178102 (2005), arxiv:cond-mat/0502397.
[15] C. P. Broedersz and F. C. MacKintosh, Reviews of Modern Physics **86**, 995 (2014), arxiv:1404.4332.
[16] A. J. Licup, S. Münster, A. Sharma, M. Sheinman, L. M. Jawerth, B. Fabry, D. a. Weitz, and F. C. MacKintosh, Proceedings of the National Academy of Sciences **112**, 9573 (2015), arxiv:1503.00924.
[17] A. Sharma, A. J. Licup, K. A. Jansen, R. Rens, M. Sheinman, G. H. Koenderink, and F. C. MacKintosh, Nature Physics **12**, 584 (2016), arxiv:1506.07792.
[18] M. Merkel and M. L. Manning, New Journal of Physics **20**, 022002 (2018).
[19] D. M. Sussman and M. Merkel, Soft Matter **14**, 3397 (2018).
[20] X. Wang, M. Merkel, L. B. Sutter, G. Erdemci-Tandogan, M. L. Manning, and K. E. Kasza, Proceedings of the National Academy of Sciences **117**, 13541 (2020), arxiv:2005.07283.
[21] M. Plischke and B. Joós, Physical Review Letters **80**, 4907 (1998).
[22] M. Dennison, M. Sheinman, C. Storm, and F. C. MacKintosh, Physical Review Letters **111**, 095503 (2013).
[23] M. C. Wigbers, F. C. Mackintosh, and M. Dennison, Physical Review E - Statistical, Nonlinear, and Soft Matter Physics **92**, 1 (2015), arxiv:1410.7860.
[24] D. M. Sussman, M. Paoluzzi, M. Cristina Marchetti, and M. Lisa Manning, EPL (Europhysics Letters) **121**, 36001 (2018), arxiv:1712.05758.
[25] F. G. Woodhouse, H. Ronellenfitsch, and J. Dunkel, Physical Review Letters **121**, 178001 (2018).
[26] L. Zhang and X. Mao, Physical Review E **93**, 1 (2016).
[27] P. Urbani, Journal of Physics A: Mathematical and Theoretical **56**, 115003 (2023).
[28] X. Mao, A. Souslov, C. I. Mendoza, and T. C. Lubensky, Nature Communications **6**, 5968 (2015).
[29] D. Z. Rocklin, V. Vitelli, and X. Mao, Folding mechanisms at finite temperature (2018), arxiv:arXiv:1802.02704.
[30] S. Chen, T. Markovich, and F. C. MacKintosh, Physical Review Letters **130**, 088101 (2023).
[31] M. Mannattil, J. M. Schwarz, and C. D. Santangelo, Physical Review Letters **128**, 208005 (2022), arxiv:2112.04279.
[32] Reference to be inserted later.
[33] A. W. Lees and S. F. Edwards, Journal of Physics C: Solid State Physics **5**, 1921 (1972).
[34] We extracted $\kappa_E \approx 0.161$ from the tension data for the athermal limit using a linear fit. The value of $\kappa_S/k_B \approx 0.0629$ was then obtained from the fit in the inset to Fig. 3a. The parameter $b_\varepsilon \approx 0.835$ describing the interaction between isotropic and shear strain was obtained from the averaged ratio G/t at $(\varepsilon, \gamma) = (0, 0)$ for $10^{-8} \leq T \leq 10^{-5}$.
[35] M. Rubinstein and R. H. Colby, *Polymer Physics* (Oxford University Press, Oxford ; New York, 2003).

[36] M. Durand, Soft Matter **18**, 3891 (2022).

[37] The network was initialized with 40×40 nodes with connectivity $z = 3.2$ [13, 38–40], were we used homogeneous spring constant $K = 1$ and rest length $L_0 = 1$. Dangling springs and isolated islands were removed and were not counted towards the connectivity z [13]. Before running the actual MC simulations, we removed any asymmetry with respect to shear strain γ by shear-stabilizing the network [9, 13]. For each strain pair (ε, γ), we first minimized the network energy to find the corresponding athermal state before running for each temperature 10 different realizations of the MC simulation. In a slight deviation from the analytical part, in the simulations, we defined the isotropic strain such that $V = (1+\varepsilon)^D V^*$. The difference is only of higher-order in ε, and thus not relevant here. For the MC simulation, we used the Metropolis–Hastings algorithm [41] with 10^{10} MC steps, where in each step we moved a single, randomly selected node. For each temperature and strain, we chose the constant node displacement such that the transition probability was ≈ 0.5. We computed the network stress tensor as the time-averaged force dipole density of the individual springs [42] and subtracted the ideal gas contribution [22, 43, 44]. The shear modulus was computed from the shear stress using the central finite difference quotient with a shear strain step of $\Delta\gamma = 2.5 \times 10^{-3}$.

[38] C. P. Broedersz and F. C. MacKintosh, Soft Matter **7**, 3186 (2011), arxiv:1009.3848.

[39] J. L. Shivers, S. Arzash, A. Sharma, and F. C. MacKintosh, Physical Review Letters **122**, 188003 (2019), arxiv:1807.01205.

[40] S. Arzash, J. L. Shivers, A. J. Licup, A. Sharma, and F. C. MacKintosh, Physical Review E **99**, 042412 (2019), arxiv:1812.08907.

[41] D. Frenkel and B. Smit, *Understanding Molecular Simulation: From Algorithms to Applications*, 2nd ed., Computational Science Series No. 1 (Academic Press, San Diego, 2002).

[42] G. K. Batchelor, Journal of Fluid Mechanics **41**, 545 (1970).

[43] E. de Miguel and G. Jackson, The Journal of Chemical Physics **125**, 164109 (2006).

[44] M. E. Tuckerman, *Statistical Mechanics: Theory and Molecular Simulation*, illustrated edition ed. (Oxford University Press, Oxford, 2010).